

Numerical Simulation of Shear Behaviour of Non- Persistent Joints under Low and High Normal Loads

Vahab Sarfarazi, Abdolhadi Ghazvinian, Wulf Schubert

Received 16-06-2015, revised 12-01-2016, accepted 14-01-2016

Abstract

In this paper, the effect of rock bridge surface on the shear behavior of planar non-persistent joints under low and high normal loads has been investigated using particle flow code in 2 Dimensions. PFC2d was calibrated with respect to the data obtained from experimental laboratory tests to ensure the conformity of the simulated numerical models response. The models consisting non-persistent joint were simulated and tested by shear loading under low and high normal loads. The discrete element simulations demonstrated that the failure pattern was mostly influenced by normal load, while the shear strength was linked to the failure pattern and failure mechanism. The failure patterns were found reasonably similar to the experimentally observed trends.

Keywords

Particle flow code · joint separation · normal load · shear and tensile cracks

Vahab Sarfarazi

Department of Mining engineering, Hamedan university of technology, Hamedan, Mardom street, P.O.B. 65155-579, Iran
e-mail: Sarfarazi@hut.ac.ir

Abdolhadi Ghazvinian

Department of Mining engineering, Tarbiat modares university, Tehran, Gisha street, P.O.B. 14115-111, Iran
e-mail: abdolhadi@yahoo.com

Wulf Schubert

Institute for Rock Mechanics and Tunnelling, Technische Universität Graz, Rechbauerstraße 12, A-8010 Graz, Austria
e-mail: schubert@tugraz.at

1 Introduction

The shear sliding of non-persistent joints are important factors in controlling the mechanical behaviour of rock masses (Einstein [1], Wong [2]). As known, it is difficult and costly to perform field tests to investigate the mechanical behavior of jointed rock masses. Therefore, laboratory tests are commonly conducted to study the influence of joint geometry configurations on the mechanical behavior of jointed blocks [3–6]. The crack initiation, propagation and coalescence of jointed specimens with less than three open flaws under uniaxial or biaxial compression [7–9] have been investigated by many researchers. In these studies, both tensile and shear cracks have been observed [7–11]. Lajtai [12, 13], tensile wing cracks were found to first appear at the tips of horizontal joints, followed by the secondary shear cracks propagating towards the opposite joint. Mughieda et al. [14] made a thorough analysis on the Fracture mechanisms of offset rock joints. Gehle and Kutter's [15] investigation on the breakage and shear behaviour of intermittent rock joints under direct shear loading condition showed that joint orientation is an important influential parameter for shear resistance of jointed rock.

In laboratory tests, it is difficult to measure the failure mechanism of rock bridge during the loading process. Numerical simulation is another common approach that has been used to investigate the failure mechanism and the mechanical behavior of non-persistent joints using techniques such as the finite element method, realistic failure processing analysis, particle flow code), displacement discontinuity method, boundary element method, distinct element method, and a hybridized indirect boundary element method) [16–22]. Particle flow code, a distinct element method first induced by Cundall and stark [23], models the mechanical behavior of rock and soils. The materials are envisioned as an assembly comprised of arbitrary spherical particles (in 3D case) or circular disks (in 2D case) in the PFC program. Kulatilake et al [24] were the pioneers in providing a realistic calibration procedure for micro-mechanical parameters of PFC3D for a contact bonded particle model. They also established a jointed rock model by using closed flaws and investigated the relation between micro-parameters and macro-

parameters, and the mechanical behavior of jointed rock model under uniaxial loading. Deleting of some particles in a PFC2D model is another way to generate joints in a bonded particle model; this procedure creates open flaws. Zhang [25] and Zhang and Wong [26, 27] studied crack initiation, propagation and coalescence using one, two or three open flaws. Many types of crack initiation and crack coalescence observed by numerical tests have been similar to the ones observed in laboratory tests. The smooth-joint is a better way to model the mechanical behavior of a joint in PFC modeling. Bahaaddini et al. [28] used the smooth-joint in a bonded particle model to investigate the effect of joint geometrical parameters on the mechanical properties of a non-persistent jointed rock mass under uniaxial compression. Many PFC users have reported the successes, failures and difficulties encountered during PFC usage. In this work, PFC2D is used to study the Shear Behaviour of Non Persistent Joints under Low and High Normal Loads.

For this purpose, using an inverse-modelling calibration approach, the laboratory results of the uniaxial, Brazilian and triaxial tests were used to obtain the estimates of the intact rock micromechanical parameters used in the simulation. A validation of the simulation was then performed by comparison between the shear behaviour of rock bridges in PFC2D and that of the non-persistent joint tested under direct shear loading in the laboratory. The validated numerical model was used to further studying the mechanical behaviour of the jointed models with different joint persistency.

2 Laboratory tests

2.1 Model Material Preparation

The model material used in preparing the intact samples and jointed blocks was a mixture of plaster (37.5 %), cement (25 %) and water (37.5 %). The procedure of mixing, casting and curing of specimens were introduced in detailed in Sarfarazi et al. [29]. The mechanical properties of the physical models are summarized in Table 1.

2.2 Preparation, Testing and Results of the rock like model consisting of non-Persistent Joints

Two specimens with different rock bridge surface of 34 cm² and 68 cm² were prepared (Fig. 1). Based on the change in the surface of the non-persistent joints, it is possible to define the joint coefficient (JC) as the ratio of the joint surface to the total shear surface, 225 cm². So this is a new and simpler property than joint persistency. The values of JC for two specimens are 0.85 and 0.7. From each specimen two similar samples were prepared and tested under two different normal loads; 0.33 MPa and 2.5 MPa which are 5% and 38% of uniaxial strength of specimen, respectively. The procedures of mixing, casting, curing and testing of the jointed block were introduced in detailed in Sarfarazi [29].

The observation results showed that the normal load influence the failure pattern of the rock bridge. Figure 2 shows the failure

patterns obtained in the direct shear tests.

When $JC = 0.85$, under low normal load (Fig. 2a), The upper tensile crack propagates through the intact portion area and the lower tensile crack develops for a short distance and then becomes stable and does not coalesce with the tip of the other joint. The surface of failure at the bridge area is tensile because no pulverized materials and evidence of shear movement were noticed. Also, polished failure surface was other evidence for splitting tensile failure.

Under high normal load (Fig. 2b), the surface of failure at the bridge area is shear because crushed materials and evidence of shear movement were noticed. Also, friction effect was other evidence for shear failure. The shear surface plane is nearly horizontal with shear loading direction. The dilation angle is zero due to smooth pattern of failure surface.

When $JC = 0.7$, under low normal load (Fig. 2c), the upper tensile crack propagates through the intact portion area and coalesces with the tip of the other joint. The surface of failure at the bridge area is tensile because no pulverized materials and evidence of shear movement were noticed. Also, polished failure surface was other evidence for splitting tensile failure.

Under high normal load (Fig. 2d), the surface of failure at the bridge area is shear because pulverized materials and evidence of shear movement were noticed. The shear surface plane is undulating with asperity angle 15°.

2.3 Numerical Unconfined Compressive Test

Figure 3a illustrates the failure patterns for numerical simulations and experimental tested samples, respectively. The failure planes experienced numerically and through laboratory testing are well matched.

Figure 3b compares the stress-strain curves obtained experimentally and numerically, respectively. These two curves are consistent in general, and the peak strengths are also similar. A comparison between numerical results and experimental measurements are presented in Table 2.

2.4 Brazilian Test

Figure 4a and b illustrate failure patterns of the numerical and experimental tested samples, respectively. Failure planes experienced numerically and with laboratory tests are well matched.

Numerical tensile strength and experimental measurements are presented in Table 2. A comparison of the brazilian experimental measurements given in Table 2 shows good agreements with those of the numerical results.

2.5 Biaxial Test

The confined and vertical stresses are applied to the specimen by activating the servo-mechanism that controls the velocities of the four confined walls. Fig. 5 shows the fracture pattern in numerical models under six different confining pressures; i.e. 0.5 MPa, 1 MPa, 1.5 MPa, 2 MPa, 2.5 MPa, 3 MPa and

Tab. 1. Property values of the intact model material determined experimentally.

value	property
6.6	Average uniaxial compressive strength (MPa)
1	Average compressive strength (MPa)
5	Average Young modulus in compression h (MPa)
0.18	Average Poisson's ratio
20.4	Internal angle of friction
2.2	Cohesion (MPa)

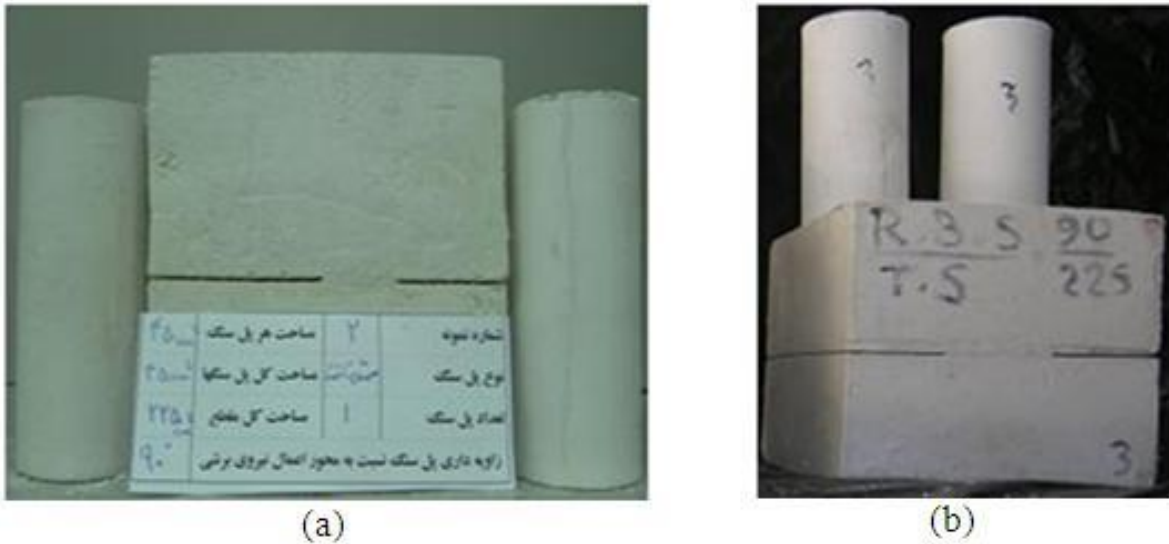


Fig. 1. The specimens with different rock bridge surfaces of a) 34 cm² and b) 68 cm²

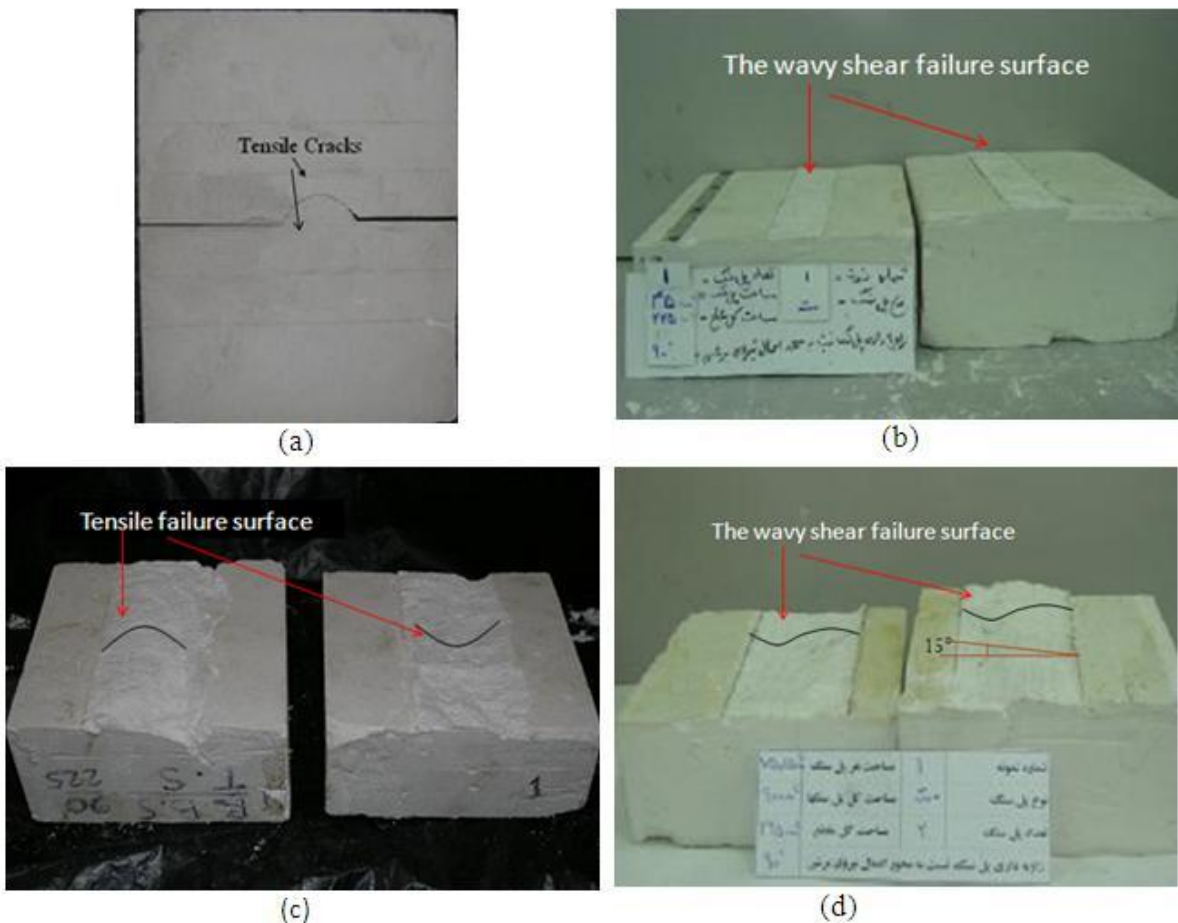


Fig. 2. The failure patterns obtained in the direct shear tests.

Tab. 2. Macro-mechanical properties of the model material in the experimental tests and PFC2D

PFC2D model results	Experimental results	Mechanical properties	PFC2D model results	Experimental results	Mechanical properties
1.1	1	Tensile strength (MPa)	5	5	Young modulus (GPa)
21	20.4	Friction angle	0.19	0.18	Poisson's ratio
2.2	2.2	Cohesion (MPa)	6.7	6.6	UCS (MPa)

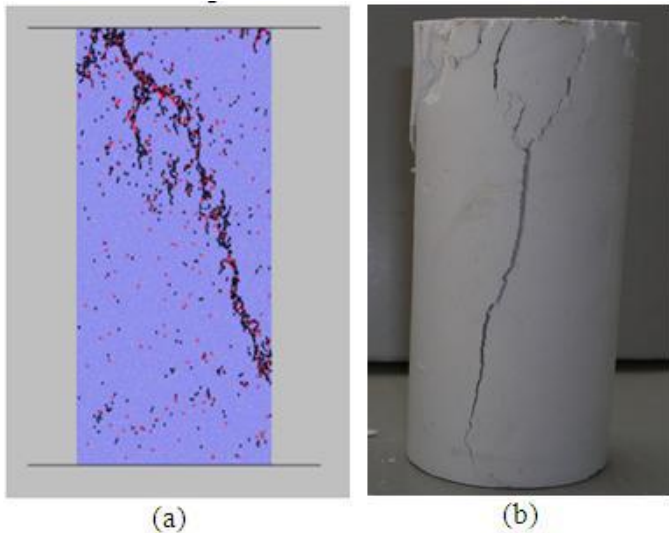


Fig. 3. a) Unconfined compressive test (cracks described by red/black lines), Ghazvinian et al. [35], b) the failure pattern in experimental testing.

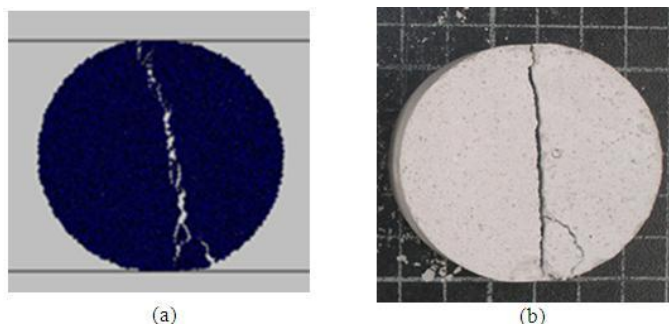


Fig. 4. The failure pattern in the a) numerical model, b) experimental samples, Ghazvinian et al. [3]

3.5 MPa. When confining pressure is 0.5 MPa, one failure surface is responsible for sample failure but when confining pressure is 3.5 MPa, several crossover failure surfaces bring sample to failure. These failure patterns are similar to the failure patterns that occurred in physical samples. A comparison of these experimental results given in Table 2 demonstrates suitably good agreement with those of the numerical measurements.

2.6 Numerical Direct Shear Tests on the Non-Persistent Open Joint

2.6.1 Preparing the Model

After calibration of PFC2D, direct shear tests for jointed rock were numerically simulated by creating a shear box model in the PFC2D (Fig. 6). The PFC specimen had the dimensions of 76 mm × 60 mm. A total of 11179 disks with a minimum ra-

dius of 0.27 mm were used to make up the shear box specimen. The particles were surrounded by four walls. The planar non-persistent joints were formed by deletion of two non-persistent vertical bands of particles from the model. The opening of these notches is 1 mm (Fig. 6). To create the shear test condition, two horizontal narrow bands of particles, with the width of 1 mm, were deleted from both the upper left side and the lower right side of the model at a distance between the joint walls and the shear box wall (Fig. 6). In total four specimens containing two planar edge-notched joints with different lengths were set up to investigate the influence of joint separation on the shear behaviour of rock bridges. For different specimens, the lengths of these edge-notched joints were different, while in the same specimen, the lengths of those two joints were the same, and they are both arrayed in the vertical middle plane. The joint length (b) has a range from 12 mm to 25.5 mm with an increment of 4.5 mm, while the joint separation or ligament length (l) decreases from 36 to 9 mm with a negative change value of 9 mm. Based on the change in the length of planar non-persistent joints, it is possible to define the joint coefficient (JC) as the ratio of the joint surface to the total shear surface, i.e. $2b / (T + 2b)$. The value of JC increases from 0.4 to 0.85 with an increment of 0.15.

2.6.2 Loading Set Up

Both the upper and left walls of the shear box were fixed (Fig. 6). Shear loading was applied to the sample by moving the lower wall in the positive Y-direction, with an adequate low velocity (i.e., 0.016 m/s) to ensure a quasi-static equilibrium, while the normal stress was kept constant by adjusting the right wall's velocity using a numerical servo-mechanism. The normal stresses applied to the rock bridges in the numerical tests was the same as in the laboratory tests (i.e., 0.3 MPa and 2.5 MPa). The shear force was registered by taking the reaction forces on the wall 2 in Fig. 6.

3 Results and Discussion

3.1 Influence of normal load on the Failure Behaviour of the Rock Bridge

Figures 7, 8, 9 and 10 illustrate the shear behaviours of rock bridge under two different normal load for $JC = 0.85, 0.7, 0.55$ and 0.4, respectively. In each figure, the fracture patterns at three stages of shear loading (i.e. at the crack initiation stress stage of I, at the peak stress of II, and after the peak shear stress of III that have been shown in these figures) have been shown. At each

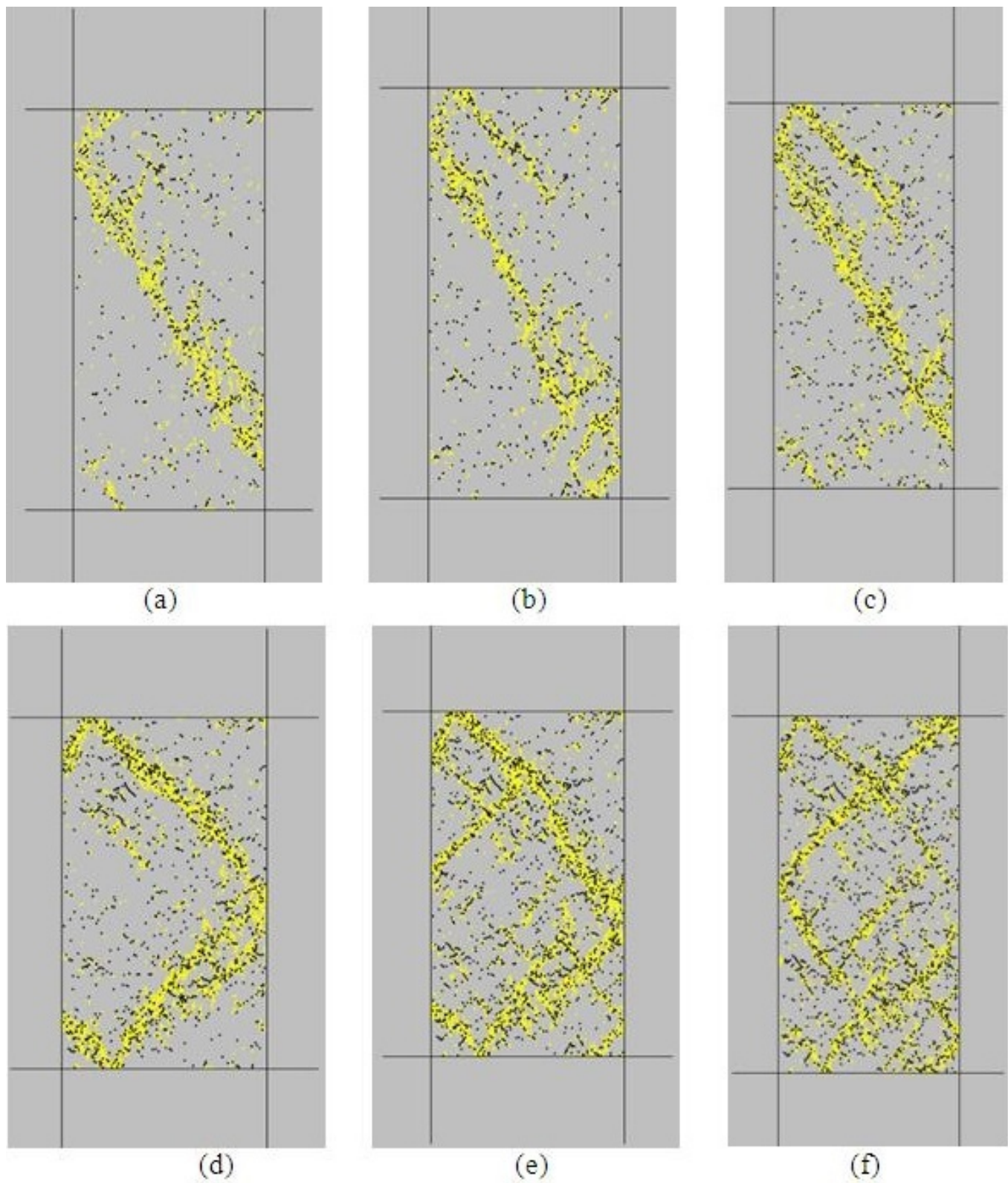


Fig. 5. The fracture pattern in numerical models, Ghazvinian et al. [3]

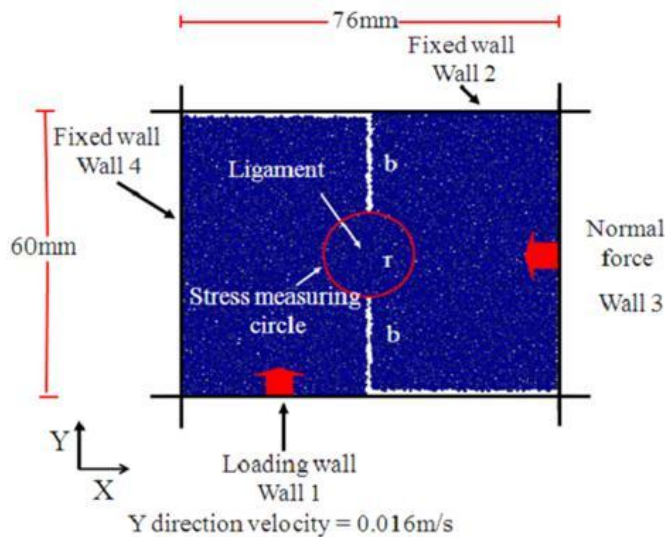


Fig. 6. Illustration of the direct shear test simulation scheme in PFC.

stage of the simulation, the crack orientation and the number of shear and tension induced cracks were determined.

3.1.1 $JC = 0.85$

Stage I: When normal load is 0.3 MPa, before the peak shear stress is reached (Fig. 7a (I)), only tensile fractures are initiated at the tip of the joints as a result of the release of tensile force. They propagate in a curvilinear path to form the so-called “wing cracks.” These cracks are categorized in the major fracture set of F1 with a mean orientation of 65.5° . Since the force intensity at the unbroken bonds is not enough to rupture the contacts, the cracks develop in a stable manner.

When normal load is 2.5 MPa, before the peak shear stress is reached (Fig. 7b (I)), only tensile fractures are initiated within the rock bridge and propagated for a short distance as a result of the release of tensile force. These cracks are categorized in the major fracture set of F1 with a mean orientation of 30° .

Stage II: When normal load is 0.3 MPa, at the peak shear stress (Fig. 7a (II)), the new tensile cracks are developed along the fracture set of F1 and propagate for a large distance. The mean orientation of the fracture set, F1, is 56.2° . The number of cracks in this step is 27 that are 32% of total number of cracks propagated in stage III. It means that when 32% of total cracks developed within the rock bridge, the shear strength is decreased and unstable crack growth is reached.

But when normal load is 2.5 MPa, at the peak shear stress (Fig. 7 b (II)), the new tensile cracks are developed along the fracture set F1 and propagate for a large distance. In this stage, four shear bands propagate within the rock bridge. The mean orientation of the fracture set, F1, is 30° . The number of cracks in this step is 53 that are 57% of total number of cracks propagated in stage c. It means that when 57% of total cracks developed within the rock bridge, the shear strength is decreased and unstable crack growth is reached.

Stage III: When normal load is 0.3 MPa (Fig. 7a(III)), a new tensile fracture set, F3, develops in the vicinity of the fracture

set of F1 and propagates out of the zone of maximum compressive force till coalescence with the joint tip. This coalescence leaves an elliptical core of intact particles. The mean orientation of the two fracture sets of F1 and F2 is 56.2° and 149.4° , respectively. The propagation length of fracture set F1 in this stage is equal to the length of F2 fracture set. As can be seen from Fig. 2a, nearly the same failure pattern has occurred in the physical sample when $JC = 0.85$.

When normal load is 2.5 MPa (Fig. 7b (III)), a new tensile fracture set of F2 develops in the vicinity of the fracture set of F1 but in opposite direction and propagates for a short distance. The propagation length of fracture set F1 in this stage is 2-3 times more than the length of F2 shear bands. The mean orientation of the two fracture sets of F1 and F2 is 30° and 320° , respectively.

As can be seen from Fig. 2b, nearly the same failure pattern has occurred in the physical sample when $JC = 0.85$.

3.1.2 $JC = 0.7$

Stage I: When normal load is 0.3 MPa (Fig. 8a (I)), the upper and lower tensile cracks (in the fracture set, F0) develop with a mean orientation of 48.8° from the notch tips and propagate for a considerable distance. Also, a few tensile cracks with the mean orientation of 27.8° (in the fracture set, F1) develop within the rock bridge. These fracture sets turn stable because of the release of tensile force with the development of tensile cracks.

When normal load is 2.5 MPa (Fig. 8b (I)), the upper and lower tensile cracks (in the fracture set, F0) develop with a mean orientation of 60° from the notch tips and propagate for a short distance.

Stage II: When normal load is 0.3 MPa (Fig. 8a (II)), the new tensile cracks which form the fracture set of F1 develop at the midst of the rock bridge. Also a few tensile cracks develop near the fracture set F0. The mean orientation of the two distinct fracture sets of F0 and F1 is 48.8° and 26.1° , respectively. The number of cracks in this step is 70 that are 41% of total number of cracks which propagate in stage III. It means that when 41% of total cracks developed within the rock bridge, the shear strength is decreased and unstable crack growth is reached.

When normal load is 2.5 MPa (Fig. 8 b (II)), the new tensile cracks which form the fracture set of F1 develops at the midst of the rock bridge. The mean orientation of fracture set of F1 is 35° . In this stage, the number of newly developed tensile cracks existing in the fracture set F1 is more than that in the fracture set F0. This means that the maximum tensile force has been transmitted within the rock bridge so several shear band develops in this area. The number of cracks in this step is 125 that are 59% of total number of cracks which propagate in stage III. It means that when 59% of total cracks developed within the rock bridge, the shear strength is decreased and unstable crack growth is reached.

Stage III: In the final stage of the shear loading, when normal load is 0.3 MPa (Fig. 8a (III)), the tensile cracks develop near the fracture set, F1. Also the tensile fracture set F2 develops within

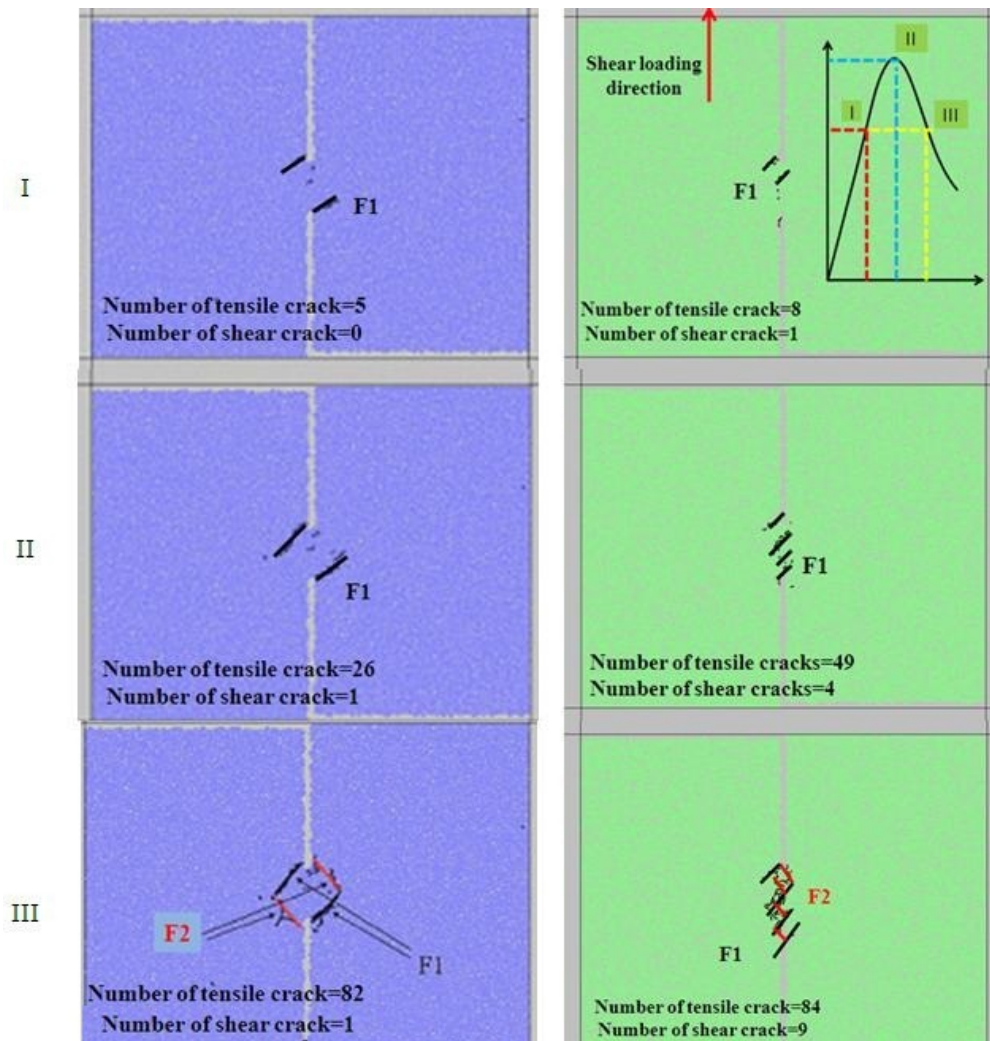


Fig. 7. Development of cracks and mean orientation of particle cracks during the three stages of shear loading of I, II and III; a) under low normal load of 0.3 MPa, b) under high normal load of 2.5 MPa.

the rock bridge and coalesces with the joint tip so that the intact bridge area gets split with an uneven shear failure surface. It is worth noting that a few shear cracks are observed in each fracture set. The mean orientation of two fracture sets, F1 and F2, is 26.1° and 158.3° , respectively. The length and orientation of fracture set F0 remain constant after the first stage. It means that the external shear load has no effect on the force concentration near the fracture set F0 after the first stage of shear loading. The propagation length of fracture set F1 in this stage is nearly equal to the length of F2 fracture set. As can be seen from Fig. 2c, nearly the same failure pattern has occurred in the physical sample when $JC = 0.7$.

Wong et al. [2] gained similar related results showing that ‘fish eye’ mode coalescence occurs in a critical range of joint coefficients ($JC = 0.7$) in experiments using plaster modelling material under direct shear tests.

When normal load is 2.5 MPa (Fig. 8b (III)), tensile cracks develop near the fracture set, F1. Also the tensile fracture set F2 develops within the rock bridge and coalesces with the fracture set F1 so that the intact bridge area fractured hardly with several shear bands. The mean orientation of two fracture sets of F1 and F2 is 40° and 330° , respectively. The propagation length

of fracture set F1 in this stage is nearly 2-3 times more than the length of F2 fracture set. The length and orientation of fracture set F0 remain constant after the first stage of shear loading. It means that the external shear load does not induce any force concentration near the fracture set F0 during the different stages of shear loading (stages of I and II) As can be seen from Fig. 2d, nearly the same failure pattern has occurred in the physical sample when $JC = 0.7$.

3.1.3 $JC = 0.55$

Stage I: When normal load is 0.3 MPa, before the peak shear stress is reached (Fig. 9a (I)), two distinct tensile fracture sets of F0 and F1 are identified in the bridge area with a mean orientation of 61.3° and 29.5° , respectively. The upper and lower tensile wing cracks (in fracture set, F0) develop at the notch tips and propagate for a short distance. Also the fracture set of F1 develops at the midst of rock bridge as several short shear bands because of the low stress interaction between the joints.

When normal load is 2.5 MPa (Fig. 9b (I)), the tensile fracture set of F1 is identified in the bridge area with a mean orientation of 45° . This fracture set initiates near the joint tips where the tensile stress concentration is high. The fracture set F1 propagates

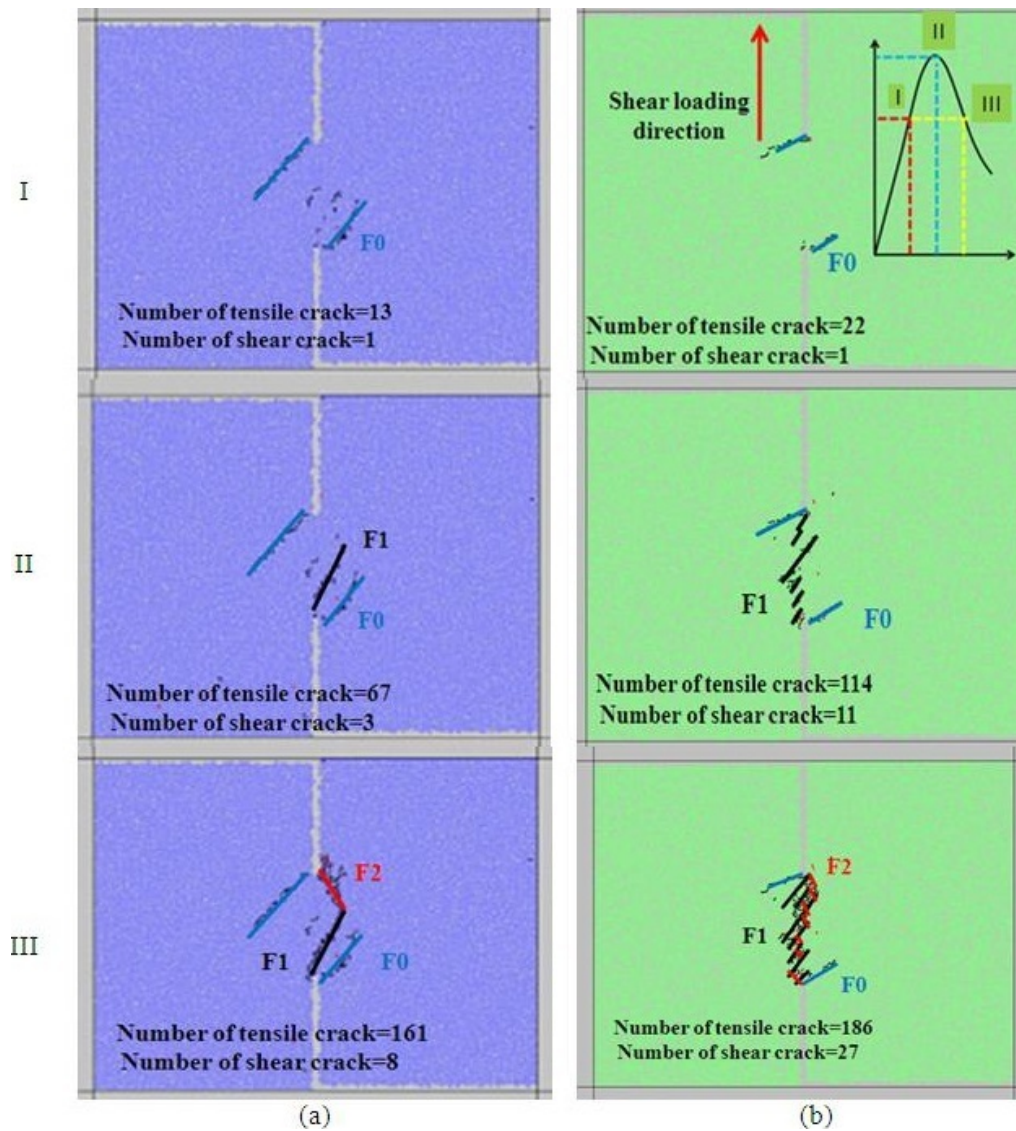


Fig. 8. Development of cracks and mean orientation of particle cracks during the three stages of shear loading of I, II and III; a) under low normal load of

0.3 MPa, b) under high normal load of 2.5 MPa.

for a short distance and become stable.

Stage II: When normal load is 0.3 MPa, as the shear stress reaches the peak strength (Fig. 9a (II)), the new tensile cracks develop along the fracture set F1, and so the shear bands propagate for a large distance. The mean orientation of fracture set F1 is equal to 25° . The numbers of cracks in this step are 109 that are 46% of total number of cracks which propagate in stage III. It means that when 46% of total cracks developed within the rock bridge, the shear strength is decreased and unstable crack growth is reached.

When normal load is 2.5 MPa (Fig. 9b (II)), the number of tensile fracture set F1 is increased. These shear bands propagate for a large distance. The mean orientation of fracture set F1 is equal to 50° . The numbers of cracks in this step are 223 that are 62% of total number of cracks which propagate in stage III. It means that when 62% of total cracks developed within the rock bridge, the shear strength is decreased and unstable crack growth is reached.

Stage III: When normal load is 0.3 MPa, in the final stage of

the shear loading (Fig. 9a (III)), the short tensile fracture set F2 develops between the shear bands so that the intact bridge area gets broken with an unsymmetrical shear failure surface. The mean orientation of fracture set F2 is 158.6° . It is important to note that only the two fracture sets of F1 and F2 are responsible for the breakage of the rock bridge. The length and orientation of fracture set F0 remain constant after the first stage of shear loading. It means that the external shear load does not induce any force concentration near the fracture set F0 during the different stages of shear loading (stages of I and II). The propagation length of fracture set F1 in this stage is nearly 1.5-2 times more than the propagation length of F2 fracture set.

When normal load is 2.5 MPa (Fig. 9b (III)), the short tensile fracture set F2 develops between the fractures set F1 so that the intact bridge area gets broken with an unsymmetrical shear failure surface. The mean orientation of fracture set F2 is 340° . The propagation length of fracture set F1 in this stage is nearly 2-3 times more than the propagation length of F2 fracture set.

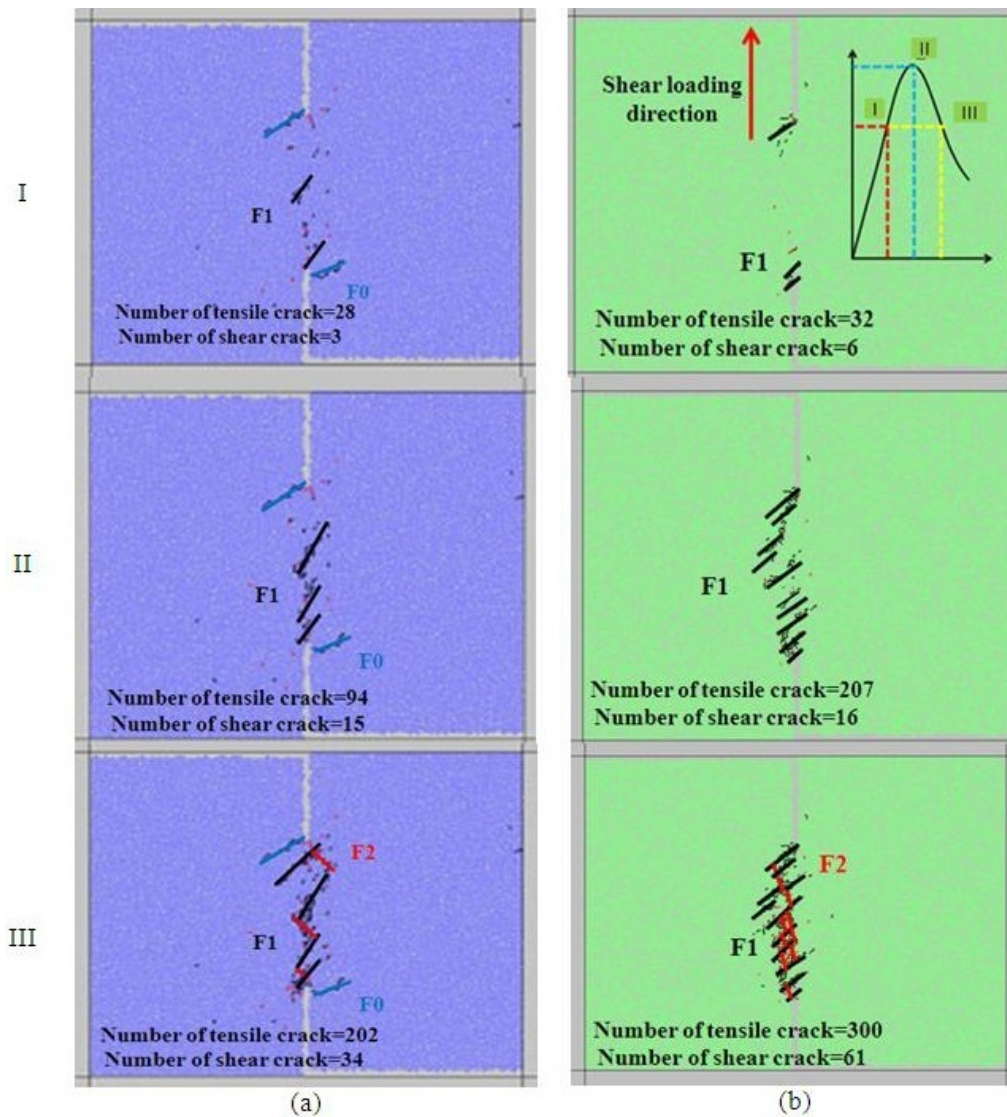


Fig. 9. Development of cracks and mean orientation of particle cracks during the three stages of shear loading of I, II and III; a) under low normal load of

0.3 MPa, b) under high normal load of 2.5 MPa.

3.1.4 $JC = 0.4$

Stage I: When normal load is 0.3 MPa (Fig. 10a (I)), both shear and tensile cracks (in fracture set F1) accumulate in the rock bridge prior to the peak shear stress being attained. It can be seen that several shear bands propagate in a stable manner for a short distance. The mean orientation of the tensile fracture set F1 is 35.1° . Unlike in the previous cases, there are no cracks at the tip of the joints in this stage. In other words, the stress concentration at the tip of the joints is not enough to overcome the bond strength, while several short bands of contacts, due to their critical situation with respect to the shear loading path, break in the rock bridge.

When normal load is 2.5 MPa (Fig. 10b (I)), the tensile fracture set F1 initiate at tip of the joint and propagate for a short distance. The mean orientation of the tensile fracture set F1 is 60° .

Stage II: When normal load is 0.3 MPa, as the shear stress reaches the peak strength (Fig. 10a (II)), new cracks (tensile/shear) develop along the fracture set F1 so the shear bands

propagate for a large distance. The mean orientation of the tensile fracture set of F1 is 30.2° . The numbers of cracks in this step are 189 that are 52% of total number of cracks which propagate in stage c. It means that when 52% of total cracks developed within the rock bridge, the shear strength is decreased and unstable crack growth is reached.

When normal load is 2.5 MPa (Fig. 10b (II)), new cracks (tensile/shear) develop parallel to the fracture set F1 for a large distance. The mean orientation of the tensile fracture set of F1 is 60° . The numbers of cracks in this step are 303 that are 66% of total number of cracks which propagate in stage c. It means that when 66% of total cracks developed within the rock bridge, the shear strength is decreased and unstable crack growth is reached.

Stage III: When normal load is 0.3 MPa, in the final stage of shear loading (Fig. 10a (III)), the short fracture set of F2 consists of both shear and tensile cracks, with a mean orientation of 156° , develops between the shear bands so that the intact bridge area gets broken with an unsymmetrical shear failure surface. The fracture set F2 is approximately symmetrical to the fracture

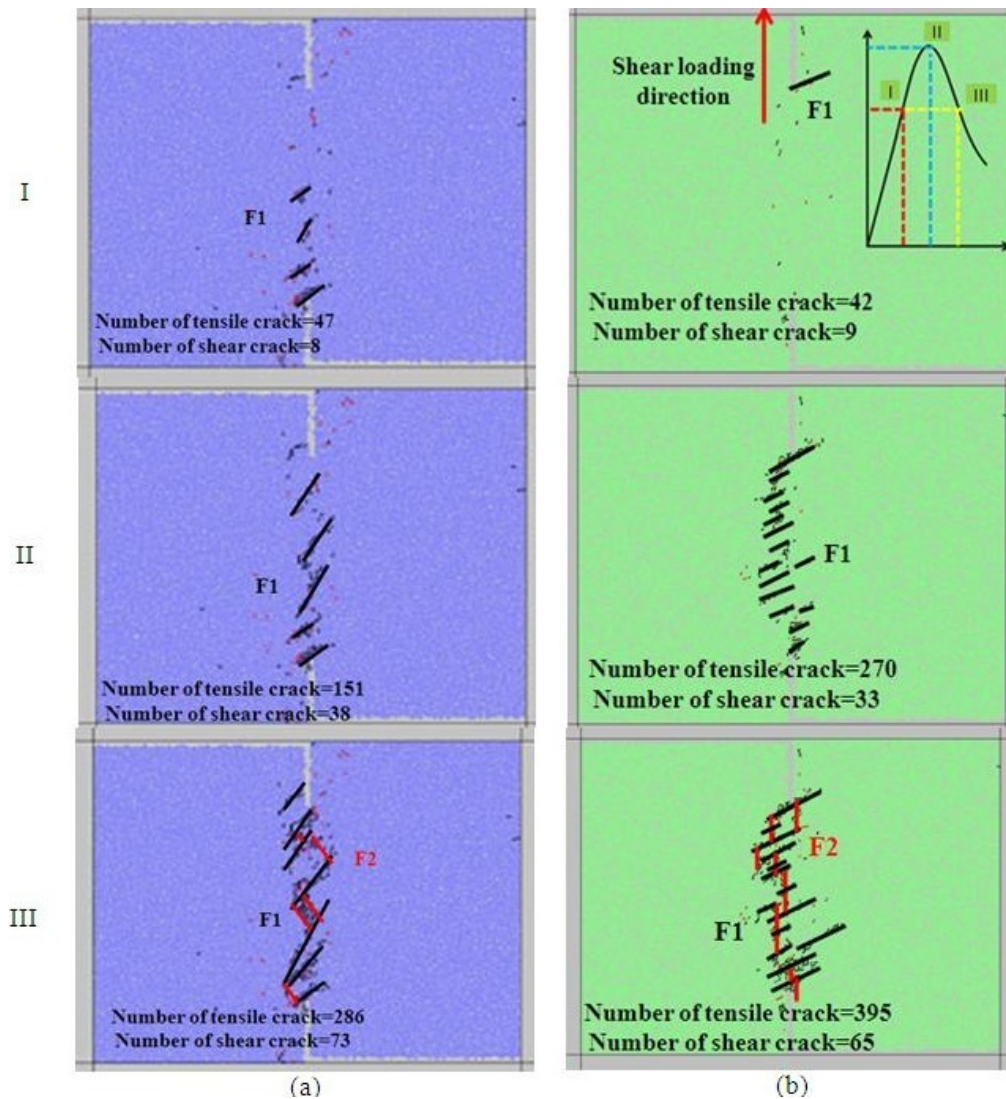


Fig. 10. Development of cracks and mean orientation of particle cracks during the three stages of shear loading of I, II and III; a) under low normal load of

0.3 MPa, b) under high normal load of 2.5 MPa.

set F1, but in the opposite direction. The propagation length of fracture set F1 in this stage is 1.5 - 2 times more than the propagation length of F2 fracture set.

When normal load is 2.5 MPa (Fig. 10b (III)), the short fracture set of F2 consists of both shear and tensile cracks develops between the shear bands so that the intact bridge area gets broken with an unsymmetrical shear failure surface. The mean orientation of the tensile fracture set of F2 is 355°. The propagation length of fracture set F1 in this stage is 2 - 3 times more than the propagation length of F2 fracture set.

The failure pattern obtained from this simulation is in reasonable accordance with some of the related numerical results in Zhang et al. [31].

From the above discussions, generally we can conclude that:

- The number of shear cracks increase by increasing in normal load therefore at the low normal load level (0.3 MPa) failure does not occur because of shear stresses, but rather from tensile stresses. At the high normal load the mixed shear /tensile stresses are responsible for bond breakage.
- In fixed JC, the number of shear band is increased by increas-

ing the normal load but their propagation length is decreased.

- In fixed JC, the mean orientation of the two fracture sets of F1 and F2 is increased by increasing the normal load
- In fixed JC, the echelon “>” shape failure surface change to non-symmetrical rough failure surface by increasing the normal load
- In fixed JC, the unstable crack growth length is increased by increasing the normal load
- The propagation length of fracture set F1 is nearly 1.5-2 times more than the propagation length of F2 fracture set under low normal load but under the high normal load, the propagation length of fracture set F1 is nearly 2-3 times more than the propagation length of F2 fracture set.
- In low normal load, the mean orientation of two fracture set F1 and F2 is nearly constant by increasing the JC. But in high normal load, the mean orientation of two fracture set F1 and F2 is increased by increasing the JC.

- In low normal load, the propagation length of two fracture sets of F1 and F2 is nearly constant by increasing the JC. But in high normal load, the propagation length of two fracture sets of F1 and F2 is increased by increasing the JC.

Figure 11a illustrates the linear fitting curve of peak shear load and joint coefficient for two different normal loads. Figure 11b shows the variation of failure stresses versus the joint coefficient for two different normal loads. Figures 11c and d represents the variation of failure stress versus the joint coefficient for both of the numerical and physical models under low normal load and high normal load, respectively. The fill points and the hollow points represent the stresses in the PFC2D models and laboratory samples, respectively.

Through comparison between Figs. 7, 8, 9, 10 and 11a, we can conclude that the capacity of bridged rock to resist shear loading has a close relationship with the failure patterns. The more the shear band number is, the more the peak of shear load is. For a large joint separation ($JC = 0.85$), the intact-bridged rock ruptures in elliptical mode with two short strias under low normal load but the intact-bridged rock ruptures with 8 number of short shear bands under high normal load. For joint separation of $JC = 0.7$, the middle bridged rock ruptures with a single uneven shear failure surface under low normal load but the bridged rock ruptures with 15 number of short shear bands under high normal load. For joint separation of $JC = 0.55$, two joints are connected with 5 large shear bands under low normal load but two joints are connected with 21 short shear bands under high normal load. Finally, for the joint separation of $JC = 0.4$, a shear zone consisting of 12 large shear bands forms the final fracture surface under low normal load but a more complex shear zone consisting of 26 short shear bands forms the final fracture surface under high normal load.

The linear fitting curve between the peak of the shear load and joint coefficient in Fig. 11a shows that the peak of shear load is almost linear to the joint coefficient. The smaller the ratio is ($JC = 0.4$), the higher the peak shear load is. Note that the increase in the loading capacity of the rock bridge is not only due to the increase in the length of rock bridge. This may also be explained by the fracture mechanics theory, which indicates that the small joint lengths are corresponding to the small values of the stress intensity factors (KI and KII). This leads to higher rock bridge strength. From the fitting equations under high normal load, $y = -2386x + 2326$ (Fig. 11a), it can be inferred that when the specimen has no pre-existing joints, the joint coefficient equals 0, and the peak of shear load is 2326 N. the shear load would be 60 N (approximately close to 0) when the ideal condition is achieved [i.e., when the joint runs through the whole specimen ($JC = 1$)]. Also, from the fitting equations under low normal load, $y = -1441.7x + 1442.3$ (Fig. 11a), it can be inferred that when the specimen has no pre-existing joints, the joint coefficient equals 0, and the peak of shear load is 1442.3 N. the shear load would be 0.6 N (approximately close to 0) when the ideal

condition is achieved [i.e., when the joint runs through the whole specimen ($JC = 1$)]. Therefore, the numerical results comply reasonably with the engineering expectation.

Figure 11b shows that the failure stress is reduced by increasing the JC. The shear strength of non-persistent joint under high normal load is more than the shear strength under low normal load. In fact, the rock compaction is increased by increasing in the normal load. The more compaction of rock leads to increasing in the shear strength.

Figure 11c and d shows that the shear strength of non-persistent joints predicted by numerical simulations are nearly similar to the results obtained by experimental tests. The slight discrepancy may be due to some small variations in the mechanical specifications of numerical and laboratory specimens (i.e., the tensile strength and friction angle given in Table 2).

Figure 12a and b shows the variation of failure stress and crack initiation stress versus the joint coefficient for two different normal loads, respectively

When normal load is 0.3 MPa (Fig. 12a), the difference between the failure stress and crack initiation stress is low what defined as brittle failure in rock mechanics. But when normal load is 2.5 MPa (Fig. 12b), the difference between the failure stress and crack initiation stress is high what defined as progressive failure in rock mechanics. This means that the brittle failure change to progressive failure by increasing the normal load.

Finally, it may be concluded that the peak of shear load of jointed rock is mostly influenced by its failure pattern, while the failure pattern of bridged rock is mainly controlled by the normal load. Whereas shear strength, as one of the material mechanical properties, has a close relationship with normal load, the capacity of jointed rock masses to resist shear loading is severely influenced by stress distribution around the rock masses.

4 Conclusions

The shear behaviour (failure pattern, failure mechanism and shear resistance) of rock specimens containing two edge joints with different joint separations was investigated under two different normal loads by PFC2D numerical simulation and verified by experimental tests. Based on the results obtained, the following conclusions drawn from this research are:

- 1 By increasing the normal load, number of shear cracks is increased but the tension is the dominant mode of failure.
- 2 The "V" shape failure surface change to non-symmetrical rough failure surface by increasing the normal load
- 3 By increasing the normal load, the numbers of the two fractures sets of F1 and F2 are increased but their length are decreased.
- 4 By increasing the normal load, the stable crack growth is increased.

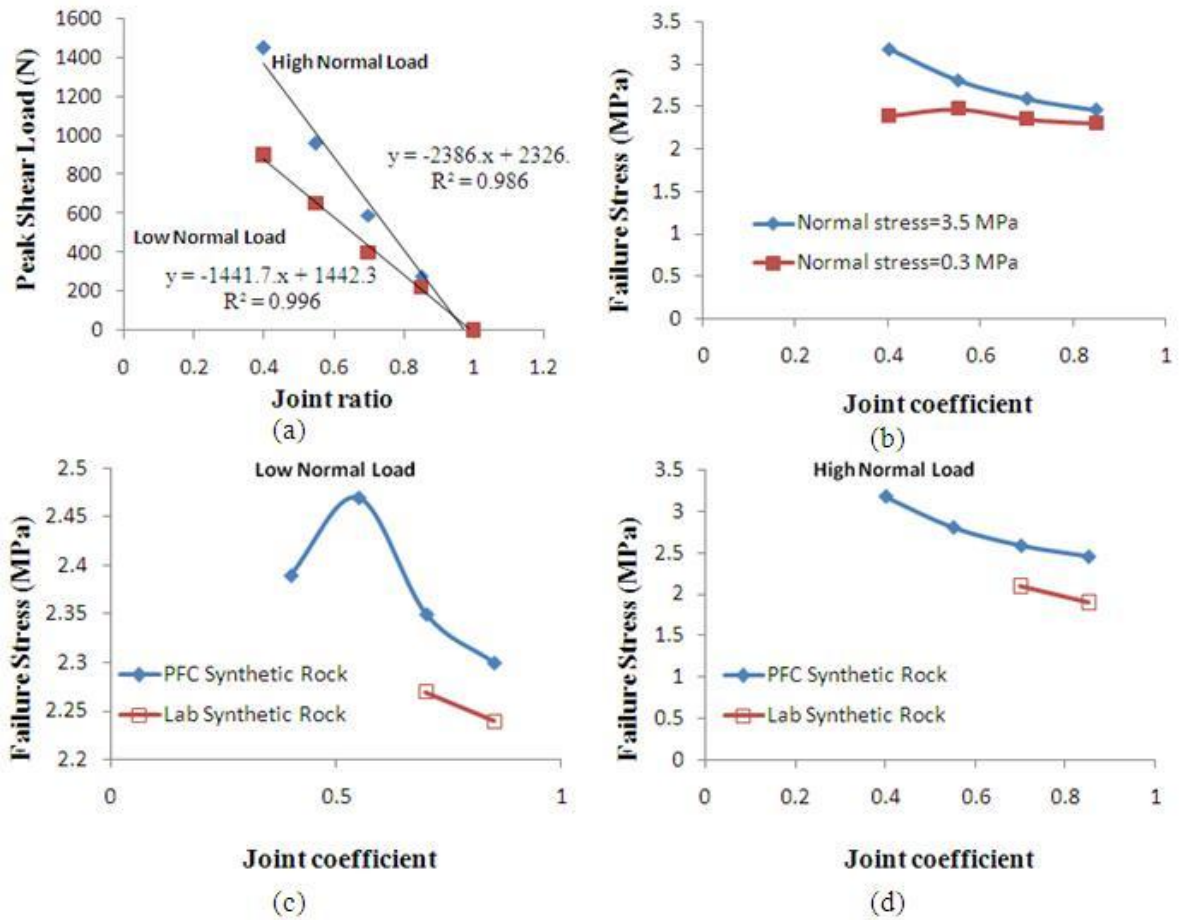


Fig. 11. a) The linear fitting curve of peak shear load and joint coefficient for two different normal loads, b) the variation of failure stress versus the joint coefficient for two different normal loads, c) the variation of failure stress versus the

joint coefficient for both of the numerical and physical models under low normal load and d) the variation of crack initiation stress versus the joint coefficient under high normal load for both of the numerical and physical models.

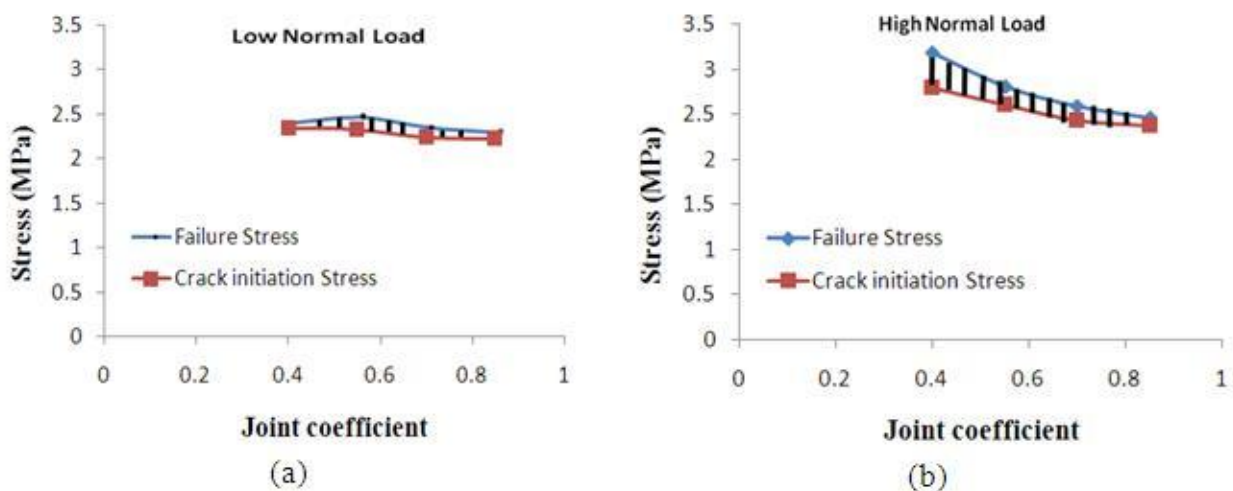


Fig. 12. The variation of failure stress and crack initiation stress versus the joint coefficient: a) under low normal load, b) under high normal load.

- 5 Brittle failure change to progressive failure by increasing the normal load.
- 6 The shear strength of non-persistent joints by numerical simulations is nearly similar to the results obtained by experimental tests.

References

- 1 **Einstein HH, Veneziano D, Baecher GB, O'Reilly KJ**, *The effect of discontinuity persistence on rock slope stability*, International Journal of Rock Mechanics and Mining Sciences & Geomechanics Abstracts, **20**(5), (1983), 227–36, DOI 10.1016/0148-9062(83)90003-7.
- 2 **Wong RHC, Chau KT**, *Crack coalescence in a rock-like material containing two cracks*, International Journal of Rock Mechanics and Mining Sciences, **35**(2), (1998), 147–164, DOI 10.1016/S0148-9062(97)00303-3.
- 3 **Yang YF, Tang CA, Xia KW**, *Study on crack curving and branching mechanism in quasi-brittle materials under dynamic biaxial loading*, International Journal of Fracture, **177**(1), (2012), 53–72, DOI 10.1007/s10704-012-9755-6.
- 4 **Sahouryeh E, Dyskin AV, Germanovich LN**, *Crack growth under biaxial compression*, Engineering Fracture Mechanics, **69**(18), (2002), 2187–2198, DOI 10.1016/S0013-7944(02)00015-2.
- 5 **Baud P, Reuschlé T, Charlez P**, *An improved wing crack model for the deformation and failure of rock in compression*, International Journal of Rock Mechanics and Mining Sciences & Geomechanics Abstracts, **33**(5), (1996), 539–542, DOI 10.1016/0148-9062(96)00004-6.
- 6 **Lajtai EZ**, *Brittle fracture in compression*, International Journal of Fracture, **10**(4), (1974), 525–536, DOI 10.1007/BF00155255.
- 7 **Wong RHC, Einstein HH**, *Crack coalescence in molded gypsum and Carrara marble: Part I. macroscopic observations and interpretation*, Rock Mechanics and Rock Engineering, **42**(3), (2009), 475–511, DOI 10.1007/s00603-008-0002-4.
- 8 **Bobet A, Einstein HH**, *Numerical modeling of fracture coalescence in a model rock material*, International Journal of Fracture, **92**(3), (1998), 221–252, DOI 10.1023/A:1007460316400.
- 9 **Tang CA, Lin P, Wong RHC, Chau KT**, *Analysis of crack coalescence in rock-like materials containing three flaws—Part II: numerical approach*, International Journal of Rock Mechanics and Mining Sciences, **38**(7), (2001), 925–939, DOI 10.1016/S1365-1609(01)00065-X.
- 10 **Chen X, Liao Z-h, Peng X**, *Cracking process of rock mass models under uniaxial compression*, Journal of Central South University, **20**(6), (2013), 1661–1678, DOI 10.1007/s11771-013-1660-2.
- 11 **De Bremaecker J-C, Ferris MC**, *Numerical models of shear fracture propagation*, Engineering Fracture Mechanics, **71**(15), (2004), 2161–2178, DOI 10.1016/j.engfracmech.2003.12.006.
- 12 **Lajtai E Z**, *Strength of discontinuous rocks in direct shear*, Geotechnique, **19**(3), (1969), 218–233, DOI 10.1680/geot.1969.19.2.218.
- 13 **Lajtai EZ**, *Shear strength of weakness planes in rock*, International Journal of Rock Mechanics and Mining Sciences & Geomechanics Abstracts, **6**(5), (1969), 499–515, DOI 10.1016/0148-9062(69)90016-3.
- 14 **Mughieda OS, Alzoubi AK**, *Fracture mechanisms of offset rock joints-A laboratory investigation*, Geotechnical and Geological Engineering, **22**(4), (2004), 545–562, DOI 10.1023/B:GEGE.0000047045.89857.06.
- 15 **Gehle C, Kutter HK**, *Breakage and shear behaviour of intermittent rock joints*, International Journal of Rock Mechanics and Mining Sciences, **40**(5), (2003), 687–700, DOI 10.1016/S1365-1609(03)00060-1.
- 16 **Chan H C M, Li V, Einstein H H**, *A hybridized displacement discontinuity and indirect boundary element method to model fracture propagation*, International Journal of Fracture, **45**(4), (1990), 263–282, DOI 10.1007/BF00036271.
- 17 **Bobet A**, *A hybridized displacement discontinuity method for mixed mode I–II–III loading*, International Journal of Rock Mechanics and Mining Sciences, **38**(8), (2001), 1121–1134, DOI 10.1016/S1365-1609(01)00081-8.
- 18 **Tang CA, Kou SQ**, *Crack propagation and coalescence in brittle materials under compression*, Engineering Fracture Mechanics, **61**(3–4), (1998), 311–324, DOI 10.1016/S0013-7944(98)00067-8.
- 19 **Tang CA, Liu H, Lee PKK, Tsui Y, Tham LG**, *Numerical studies of the influence of microstructure on rock failure in uniaxial compression — Part I: effect of heterogeneity*, International Journal of Rock Mechanics and Mining Sciences, **37**(4), (2000), 555–569, DOI 10.1016/S1365-1609(99)00121-5.
- 20 **Tang CA, Tham LG, Lee PKK, Tsui Y, Liu H**, *Numerical studies of the influence of microstructure on rock failure in uniaxial compression — Part II: constraint, slenderness and size effect*, International Journal of Rock Mechanics and Mining Sciences, **37**(4), (2000), 571–583, DOI 10.1016/S1365-1609(99)00122-7.
- 21 **Zhang H, He Y, Han L, Jiang B, Liang Z, Zhong S**, *Microfracturing characteristics in brittle material containing structural defects under biaxial loading*, Computational Materials Science, **46**(3), (2009), 682–686, DOI 10.1016/j.commatsci.2009.05.015.
- 22 **Mughieda O, Karasneh I**, *Coalescence of offset rock joints under biaxial loading*, Geotechnical and Geological Engineering, **24**(4), (2006), 985–999, DOI 10.1007/s10706-005-8352-0.
- 23 **Cundall PA, Strack ODL**, *A discrete numerical model for granular assemblies*, Geotechnique, **29**(1), (1979), 47–65, DOI 10.1680/geot.1979.29.1.47.
- 24 **Kulatilake PHSW, Malama B, Wang J**, *Physical and particle flow modeling of jointed rock block behavior under uniaxial loading*, International Journal of Rock Mechanics and Mining Sciences, **38**(5), (2001), 641–657, DOI 10.1016/S1365-1609(01)00025-9.
- 25 **Zhang X-P, Wong LNY**, *Cracking Processes in Rock-Like Material Containing a Single Flaw Under Uniaxial Compression: A Numerical Study Based on Parallel Bonded-Particle Model Approach*, Rock Mechanics and Rock Engineering, **45**(5), (2011), 711–737, DOI 10.1007/s00603-011-0176-z.
- 26 **Zhang X-P, Wong LNY**, *Crack Initiation, Propagation and Coalescence in Rock-Like Material Containing Two Flaws: a Numerical Study Based on Bonded-Particle Model Approach*, Rock Mechanics and Rock Engineering, **46**(5), (2013), 1001–1021, DOI 10.1007/s00603-012-0323-1.
- 27 **Bahaaddini M, Sharrock G, Hebblewhite BK**, *Numerical investigation of the effect of joint geometrical parameters on the mechanical properties of a non-persistent jointed rock mass under uniaxial compression*, Computers and Geotechnics, **49**, (2013), 206–225, DOI 10.1016/j.compgeo.2012.10.012.
- 28 **Lee H, Jeon S**, *An experimental and numerical study of fracture coalescence in pre-cracked specimens under uniaxial compression*, International Journal of Solids and Structures, **48**(6), (2011), 979–999, DOI 10.1016/j.ijsolstr.2010.12.001.
- 29 **Sarfarazi V, Ghazvinian A, Schubert W, Blumel M, Nejati HR**, *Numerical Simulation of the Process of Fracture of Echelon Rock Joints*, Rock Mechanics and Rock Engineering, **47**(4), (2014), 1355–1371, DOI 10.1007/s00603-013-0450-3.
- 30 **Ghazvinian A, Sarfarazi V, Schubert W, Blumel M**, *A Study of the Failure Mechanism of Planar Non-Persistent Open Joints Using PFC2D*, Rock Mechanics and Rock Engineering, **45**(5), (2012), 677–693, DOI 10.1007/s00603-012-0233-2.
- 31 **Zhang HQ, Zhao ZY, Tang CA, Song L**, *Numerical study of shear behavior of intermittent rock joints with different geometrical parameters*, International Journal of Rock Mechanics and Mining Sciences, **43**(5), (2006), 802–816, DOI 10.1016/j.ijrmms.2005.12.006.